Elevated intraocular pressure decreases response sensitivity of inner retinal neurons in experimental glaucoma mice

Ji-Jie Pang, Benjamin J. Frankfort, Ronald L. Gross[1], and Samuel M. Wu[2]

Cullen Eye Institute, Baylor College of Medicine, Houston, TX 77030

Edited by John E. Dowling, Harvard University, Cambridge, MA, and approved January 22, 2015 (received for review October 17, 2014)

Glaucoma is the second leading cause of blindness in the United States and the world, characterized by progressive degeneration of the optic nerve and retinal ganglion cells (RGCs). Glaucoma patients exhibit an early diffuse loss of retinal sensitivity followed by focal loss of RGCs in sectored patterns. Recent evidence has suggested that this early sensitivity loss may be associated with dysfunctions in the inner retina, but detailed cellular and synaptic mechanisms underlying such sensitivity changes are largely unknown. In this study, we use whole-cell voltage-clamp techniques to analyze light responses of individual bipolar cells (BCs), AII amacrine cells (AIIACs), and ON and sustained OFF alpha-ganglion cells (ONαGCs and sOFFαGCs) in dark-adapted mouse retinas with elevated intraocular pressure (IOP). We present evidence showing that elevated IOP suppresses the rod ON BC inputs to AIIACs, resulting in less sensitive AIIACs, which alter AIIAC inputs to ONαGCs via the AIIAC→cone ON BC→ONαGC pathway, resulting in lower ONαGC sensitivity. The altered AIIAC response also reduces sOFFαGC sensitivity via the AIIAC→sOFFαGC chemical synapses. These sensitivity decreases in αGCs and AIIACs were found in mice with elevated IOP for 3–7 wk, a stage when little RGC or optic nerve degeneration was observed. Our finding that elevated IOP alters neuronal function in the inner retina before irreversible structural damage occurs provides useful information for developing new diagnostic tools and treatments for glaucoma in human patients.

intraocular pressure | glaucoma | ganglion cells | bipolar cells | AII amacrine cells

Glaucoma is a leading cause of irreversible blindness in the United States and the world (1, 2), and is characterized by optic nerve cupping (thinning of the neuroretinal rim at the optic nerve head) and progressive optic nerve and retinal ganglion cell (RGC) degeneration as well as functional deficit revealed by psychophysical tests (3, 4). Although factors causing the eventual RGC death and blindness remain controversial (1, 5–8), increasing evidence from human patients and animal models has shown that the disease is associated with an early mild diffuse loss of retinal sensitivity or inner retinal response decrease (9–14). Although it is unclear whether these functional changes are a prelude or even causal to RGC death and blindness, elucidating the underlying synaptic and cellular mechanisms for such sensitivity/response decline will nevertheless provide novel insights pertaining to early detection and treatment of human glaucoma.

Multiple risk factors are associated with glaucomatous diseases, among which elevated intraocular pressure (IOP) is widely accepted as the most significant for both disease onset and progression (2, 15). Because high IOP (H-IOP) is an important risk factor, many experimental animal models of elevated IOP have been developed in multiple species including monkeys, rats, and mice (16–22). Most experiments performed in animal models have focused on anatomical and histopathological analyses of RGC death, axon loss, and changes to axonal projections to higher visual centers in the brain (23–25). Only a few studies have attempted to address whether function and light sensitivity of retinal neurons are affected. Some reports have suggested a possible but inconclusive involvement of amacrine cells (26, 27). A recent study examining the scotopic threshold responses (STRs) in an elevated IOP mouse model generated by the microbead occlusion method (28) has suggested that the voltage gains (ratio of post/presynaptic signals) of the negative STR [possibly representing AII amacrine cell (AIIAC) responses (29)] and positive STR [possibly representing ON GC responses (30)] are both reduced at stages before morphological changes or RGC death occurs (12). However, no changes in single RGC or their presynaptic bipolar cell (BC)/AIIAC responses have been reported in experimental glaucoma models. Studies using electroretinogram, STR, and optic nerve recording techniques lack the power to identify or establish cellular and synaptic sites of retinal dysfunction (27, 31, 32), leaving a disabling gap preventing us from knowing how elevated IOP affects light responses of individual retinal neurons. In this study, we fill this gap by using whole-cell voltage-clamp techniques to study light responses of individual alpha-RGCs (αGCs) and AIIACs, as well as their presynaptic BCs, in two experimental glaucoma mouse models.

It has been shown that light responses of mammalian AIIACs are mediated by rod bipolar cell (DBC_R) inputs via a 6,7-dinitroquinoxaline-2,3-dione (DNQX)–sensitive glutamatergic synapse and certain types of cone depolarizing bipolar cell [$DBC_{R/MC}$; ON bipolar cells with mixed rod and M-cone inputs (33), or B6-7] input via a connexin36 (Cx36)-dependent electrical synapse (34–36). AIIACs are perhaps the most sensitive (with the lowest response threshold) neurons in the mouse retina (37, 38), and thus they send highly sensitive output signals to postsynaptic neurons such as certain types of cone hyperpolarizing bipolar cells [$HBC_{R/MC}$s; OFF bipolar cells with mixed rod and M-cone inputs (39), or B1-2] and OFF GCs (37, 40). ON and sustained

Significance

Glaucoma is a leading cause of blindness, associated with elevated intraocular pressure (IOP) and progressive loss of the optic nerve and retinal ganglion cells (RGCs). Glaucoma patients exhibit diffuse loss of visual sensitivity, but the cellular origins of such sensitivity loss is unknown. In this study, we present evidence showing that elevated IOP decreases the efficacy of the rod bipolar cell to the AII amacrine cell synapse, resulting in reduction of RGC sensitivity. These findings, for the first time to our knowledge, identify the synaptic loci mediating visual sensitivity loss in early glaucoma, and can be used to develop new diagnostic tools and treatments for this blinding disease.

Author contributions: J.-J.P., B.J.F., R.L.G., and S.M.W. designed research; J.-J.P. and S.M.W. performed research; B.J.F. and R.L.G. contributed new reagents/analytic tools; J.-J.P. and S.M.W. analyzed data; and S.M.W. wrote the paper.

The authors declare no conflict of interest.

This article is a PNAS Direct Submission.

[1]Present address: West Virginia University Eye Institute, Morgantown, WV 26506.

[2]To whom correspondence should be addressed. Email: swu@bcm.edu.

OFF alpha-GCs (ONαGCs and sOFFαGCs) are two primary types of GCs in the mouse retina, and their synaptic circuitries include many major types of mammalian BCs and ACs (40–42). By studying the effects of elevated IOP on these GCs and their presynaptic neurons, we will be able to gain insights into general mechanisms underlying inner retina dysfunction in glaucoma. ONαGCs and sOFFαGCs exhibit characteristic morphology (large somas and dendritic trees) and light response signatures (40). ONαGCs have no or very little spike activity in darkness, increased spikes in light, inward light-evoked cation current (ΔI_C; mediated by $DBC_{R/MC}$ inputs), and outward light-evoked chloride current (ΔI_{Cl}; mediated by AC inputs) (40, 43). sOFFαGCs exhibit maintained spike activity in darkness, sustained decrease of spikes in light, outward ΔI_C (mediated by $HBC_{R/MC}$ inputs), and outward ΔI_{Cl} (mediated by AIIAC/AC inputs) (40, 44). Fig. 1 is a schematic diagram of synaptic connections between ONαGCs/sOFFαGCs and their primary presynaptic neurons: DBC_Rs, $DBC_{R/MC}$s, $HBC_{R/MC}$s, and AIIACs (key synapses are labeled 1–5 in the figure; see below). In this report, we analyzed light responses of these retinal neurons in treated mice (in which H-IOP was induced; *Materials and Methods*) and compared them with the corresponding responses measured in nontreated mice with normal IOP (n-IOP).

Results

Effects of Elevated IOP on Light-Evoked Spike Responses and Cation and Chloride Currents in ON and OFF Ganglion Cells. We first studied how elevated IOP affects light-evoked spike responses and the BC and AC inputs (represented by ΔI_Cs and ΔI_{Cl}s, respectively) to ON and OFF GCs. Fig. 2 shows the light-evoked spike activities (Fig. 2*B*) and ΔI_C and ΔI_{Cl} (Fig. 2 *C* and *D*, respectively) of an ONαGC to light steps of various intensities in a dark-adapted flat-mounted retina of a mouse with 5-wk elevated IOP (15–24 Hg) (12, 16). The average response–intensity (R-Log I) relations of six ONαGCs in H-IOP mouse retinas (with 3- to 7-wk elevated IOP, four with the laser method and two with the microbead method; *Materials and Methods*) are shown as dotted curves in Fig. 2*E*, whereas the corresponding R-Log I relations obtained from ONαGCs in n-IOP (10–15 Hg) mice ($n = 18$) are shown as solid curves for comparison. ONαGCs were initially identified by their characteristic large soma size in flat-mounted retinas, their characteristic spike, ΔI_C, and ΔI_{Cl} response waveforms (40), and subsequently confirmed by their characteristic morphology [including soma size, dendritic pattern in the flat mount, and levels of stratification by *z*-axis rotation (40, 45, 46)] revealed by neurobiotin (NB) or Lucifer yellow (LY)

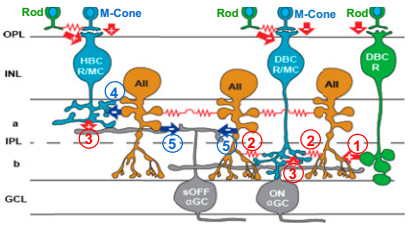

Fig. 1. Schematic diagram of major synaptic connections in the ON and OFF α-ganglion pathways in the mouse retina. Green, rods and rod BCs; blue, M cones and mixed rod/M-cone BCs; orange, AIIACs; gray, αGCs; arrows, chemical synapses (red, glutamatergic; blue, glycinergic; +, sign-preserving; –, sign-inverting); zigzag (red), electrical synapses. a, sublamina a; b, sublamina b; GCL, ganglion cell layer; INL, inner nuclear layer; IPL, inner plexiform layer; OPL, outer plexiform layer; PRL, photoreceptor layer. Synapses directly relevant to this study are marked with numbers in circles: 1: DBC_R→AIIAC glutamatergic; 2: DBC_C↔AIIAC electrical; 3: $DBC_{R/MC}$/$HBC_{R/MC}$→ONαGC/sOFFαGC glutamatergic; 4: AIIAC→$HBC_{R/MC}$ glycinergic; and 5: AIIAC→sOFFαGC glycinergic.

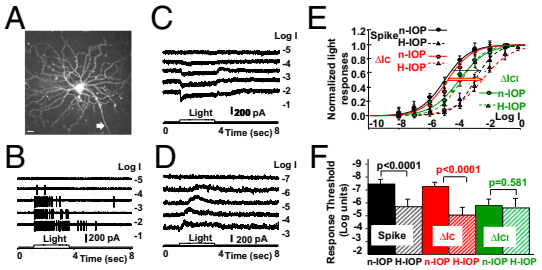

Fig. 2. Light responses of ONαGCs in high-IOP and normal-IOP mice. (*A*) Confocal image of an LY-filled ONαGC in an H-IOP mouse (white arrow, axon). (Scale bar, 20 μm.) (*B–D*) The cell's light-evoked spike responses, cation current, and chloride current to 500-nm light steps of various intensities are shown in *B–D*, respectively. (*E*) The normalized, average response–intensity relations of six ONαGCs in H-IOP mice [population R_{max} (mean ± SE) for spike, ΔI_C, and ΔI_{Cl} responses: 88 ± 37 per s, 203 ± 16 pA, and 194 ± 18 pA] are shown as dotted curves, whereas the corresponding R-Log I relations obtained from ONαGCs in normal mice [$n = 18$, population R_{max} (mean ± SE) for spike, ΔI_C, and ΔI_{Cl} responses: 97 ± 42 per s, 218 ± 21 pA, and 183 ± 13 pA) are shown as solid curves for comparison. Black, spike responses; red, ΔI_C; green, ΔI_{Cl}. Arrows indicate H-IOP–induced shifts of the R-Log I relations. (*F*) Bar graphs of the average light response thresholds (mean ± SE), defined as the light intensity eliciting 5% of the maximum response of spike responses, ΔI_C, and ΔI_{Cl} in control and H-IOP mouse retinas; the significance levels of the threshold differences are given by the *P* values of the *t* test.

fluorescence after the experiment (Fig. 2*A*). It is evident from Fig. 2*E* that light-evoked spike responses and ΔI_C of ONαGCs in the H-IOP retina (black and red dotted curves) are about 2 log units less sensitive (right shifts of the R-Log I curves; thin black arrow and thick red/yellow arrow) than the corresponding responses of the ONαGCs in n-IOP mice (black and red solid curves). The average light response thresholds, defined as the light intensity eliciting 5% of the maximum response, of spike responses, ΔI_C, and ΔI_{Cl} in n-IOP and H-IOP mouse retinas are shown as bar graphs in Fig. 2*F*. The differences in spike and ΔI_C thresholds between the H-IOP and n-IOP mice are highly significant ($P < 0.0001$, *t* test), and the difference in ΔI_{Cl} thresholds between the two groups is not ($P = 0.581$). The ONαGC spike responses in both n-IOP and H-IOP retinal groups are close to ΔI_C but not to ΔI_{Cl} (Fig. 2*E*, solid and dashed green curves), suggesting the spike responses of the mouse ONαGCs are largely mediated by the DBC_C inputs. One reason for this is that the dark resting potential of mouse ONαGCs is very close to chloride equilibrium potential (E_{Cl}) (40), and thus ΔI_{Cl} contributes very little to the spike generator potentials due to lack of driving force. In view of the anatomical and physiological evidence that $DBC_{R/MC}$s are strongly coupled with AIIACs (47, 48), it is possible that the H-IOP–induced spike response sensitivity decrease is mediated by the AIIAC→$DBC_{R/MC}$s→ONαGC (ΔI_C) pathway (synapses 2 and 3 in Fig. 1).

Fig. 3 shows the morphology in the flat-mounted retina (Fig. 3*A*), light-evoked spike activities (Fig. 3*B*), and ΔI_C and ΔI_{Cl} (Fig. 3 *C* and *D*, respectively) of an sOFFαGC to light steps of various intensities, and the average R-Log I relations of 7 sOFFαGCs in the H-IOP (15–25 Hg; 4 with the laser method and 3 with the microbead method; *Materials and Methods*) mice and 15 sOFFαGCs in the n-IOP (10–15 Hg) mice (Fig. 3*E*). sOFFαGCs were identified in similar ways as for the ONαGCs described above and in previous publications (including characteristic light responses, soma size, dendritic pattern, and the inner plexiform layer levels of stratification) (40, 42). The light-evoked spike responses and ΔI_{Cl} of the sOFFαGCs in H-IOP retinas (Fig. 3*E*, black and red dashed curves) are 2 log units less sensitive than the corresponding responses of the sOFFαGCs in the n-IOP mice (black and red dashed curves; thin black arrow and thick green/yellow arrow). sOFFαGCs in n-IOP retinas show

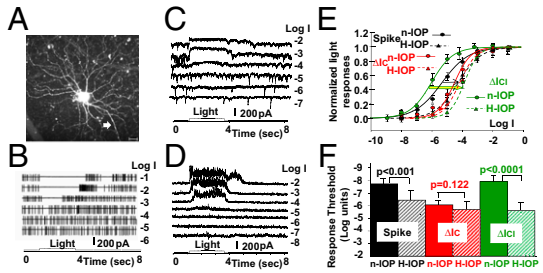

Fig. 3. Light responses of sOFFαGCs in H-IOP and n-IOP mice. (*A*) Confocal image of an LY-filled sOFFαGC in an H-IOP mouse (white arrow, axon). (Scale bar, 20 μm.) (*B–D*) The cell's light-evoked spike responses, ΔI_C, and ΔI_{Cl} to 500-nm light steps of various intensities are shown in *B–D*, respectively. (*E*) The normalized, average R-Log I relations of seven sOFFαGCs in H-IOP mice [population R_{max} (mean ± SE) for spike, ΔI_C, and ΔI_{Cl} responses: 12 ± 8 per s, 181 ± 15 pA, and 250 ± 25 pA] are shown as dotted curves, whereas the corresponding R-Log I relations obtained from sOFFαGCs in n-IOP mice [n = 15, population R_{max} (mean ± SE) for spike, ΔI_C, and ΔI_{Cl} responses: 14 ± 8 per s, 162 ± 16 pA, and 241 ± 33 pA) are shown as solid curves for comparison. Black, spike responses; red, ΔI_C; green, ΔI_{Cl}. Colored arrows indicate H-IOP–induced shifts of the R-Log I relations. (*F*) Bar graphs of the average light response thresholds (mean ± SE) of spike responses, ΔI_C, and ΔI_{Cl} in n-IOP and H-IOP mouse retinas; the significance levels of the threshold differences are given by the *P* values of the *t* test.

that the average spike R-Log I curve (black solid curve) lies between the average ΔI_{Cl} R-Log I (solid green) and the ΔI_C R-Log I (solid red), with the low-intensity ends very close to the ΔI_{Cl} R-Log I. The average light response thresholds of spike responses, ΔI_C, and ΔI_{Cl} in n-IOP and H-IOP mouse retinas are shown as bar graphs in Fig. 3*F*. The differences in spike and ΔI_{Cl} thresholds between the H-IOP and n-IOP mice are highly significant ($P < 0.001$, *t* test), and the difference in ΔI_C thresholds between the two groups is not ($P = 0.122$). These results suggest that the spike responses of mouse sOFFαGCs at low light intensities are largely mediated by an AC input of high sensitivity. The most likely ACs with such high sensitivity are the AIIACs (37, 38). The reason why both the ΔI_C and ΔI_{Cl} contribute to the sOFFαGC spike activity is that the dark resting potential of the mouse sOFFαGCs is about 10 mV positive to E_{Cl} (in contrast to the near E_{Cl} dark membrane potential of the ONαGCs described in Fig. 2) (40), and thus both ΔI_C and ΔI_{Cl} have enough driving force to contribute to the spike generator potentials in sOFFαGCs. Because AIIACs make chemical synapses on sOFFαGCs (synapse 5 in Fig. 1) (40, 44), it is possible that the H-IOP–induced sOFFαGC ΔI_{Cl} and spike response sensitivity decreases are mediated by AIIACs.

Elevated IOP Does Not Significantly Alter the ON and OFF Bipolar Cell Light Sensitivities. We next examined the effects of elevated IOP on the three types of BCs presynaptic to ONαGCs and sOFFαGCs: the $HBC_{R/MC}$, $DBC_{R/MC}$, and DBC_R (synapses 3 and 1 in Fig. 1). Fig. 4*A* shows the morphology and ΔI_C of an $HBC_{R/MC}$, $DBC_{R/MC}$, and DBC_R to light steps of various intensities in dark-adapted living retinal slices of mice with 5-, 3-, and 7-wk elevated IOP (17–24 Hg), respectively. Retinal slices such as that shown in the left panel (DBC_R) were counterstained with the anti-PKCα antibody [red; labels all DBC_Rs (33)] to demonstrate that the recorded cells were DBC_Rs. The $HBC_{R/MC}$ and $DBC_{R/MC}$ were identified by their characteristic morphology (including soma size/shape and patterns/levels of axon terminal stratification), response waveforms, thresholds, and dynamic ranges (33, 39). The average R-Log I relations of 4 $HBC_{R/MC}$s, 3 $DBC_{R/MC}$s, and 5 DBC_Rs in H-IOP mouse retinas (with 3- to 7-wk elevated IOP, 16–24 Hg, 2 $HBC_{R/MC}$s, 1 $DBC_{R/MC}$, and 2 DBC_Rs with the laser method and 2, 2, and 3 with the microbead method; *Materials and Methods*) are shown as dotted curves in Fig. 4*C*, whereas the corresponding R-Log I relations obtained from 7 $HBC_{R/MC}$s, 6 $DBC_{R/MC}$s, and 11 DBC_Rs in n-IOP mice are shown as solid curves for comparison. The average light response thresholds of ΔI_C of the three types of BCs in n-IOP and H-IOP mouse retinas are shown as bar graphs in Fig. 4*D*. The differences in $HBC_{R/MC}$, $DBC_{R/MC}$, and DBC_R ΔI_C thresholds between the H-IOP and n-IOP mice are not significant ($P = 0.667$, 0.422, and 0.180, respectively, *t* test). Because dark resting potentials of the mouse BCs are very close to E_{Cl} (37), the light-evoked voltage responses of the three types of BCs are mainly derived from the ΔI_C contribution. Therefore, the BC responses presynaptic to ONαGC and sOFFαGC ΔI_C are not significantly altered by elevated IOP.

Elevated IOP Suppresses Rod Bipolar Cell Synaptic Inputs to AIIACs. Because results in Figs. 2 and 3 suggest that the H-IOP–induced sensitivity loss in ON and OFF GCs is likely to be mediated by AIIACs, we examined light-evoked rod and cone DBC (DBC_Rs and DBC_Cs) inputs to AIIACs (synapses 1 and 2 in Fig. 1) in mice with elevated IOP. Fig. 5 shows the confocal image and light responses of an AIIAC in an H-IOP mouse with 3 wk of elevated IOP. Similar to the AIIACs recorded in retinal slices of the n-IOP mice (34, 37), AIIACs in retinal slices of H-IOP mice are reasonably well clamped. The current–voltage responses and cation current responses (ΔI_C) to 500-nm light steps of various intensities in control solution, in the presence of 100 μM DNQX [an AMPA/kainate receptor blocker that suppresses DBC_R inputs to AIIACs (34)], and in the presence of 100 μM DNQX + 100 μM MFA [meclofenamic acid; a gap-junction blocker that suppresses DBC_C inputs to AIIACs (48–50)] are shown in Fig. 5 *B–E*, respectively. The average R-Log I relations measured under various conditions in H-IOP mice are plotted as dashed curves in Fig. 5*F*; numbers of AIIACs under each condition in H-IOP mice (3–7 wk of elevated IOP, 15–22 Hg, four with the laser method and two with the microbead method; *Materials and Methods*) are given in the Fig. 5 legend, and all AIIACs were identified by their characteristic morphology and light responses (34, 37). By comparing these R-Log I relations with the corresponding results from AIIACs in n-IOP mice (34), it is evident that the AIIACs in the H-IOP mice exhibit lower light sensitivity than the AIIACs in the n-IOP mice. We also applied 100 μM

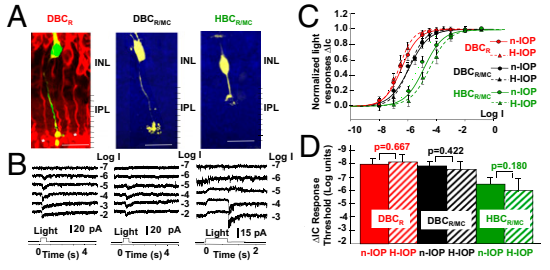

Fig. 4. Light responses of $HBC_{R/MC}$s, $DBC_{R/MC}$s, and DBC_Rs in H-IOP and n-IOP mice. (*A*) Confocal images of an LY-filled (yellow) $HBC_{R/MC}$, $DBC_{R/MC}$, and DBC_R in dark-adapted living retinal slices of mice with elevated IOP (retinal slices with DBC_Rs were counterstained with anti-PKCα; red). (Scale bars, 20 μm.) (*B*) ΔI_C to 500-nm light steps of various intensities. (*C*) Normalized, average R-Log I relations of 4 $HBC_{R/MC}$s (green), 3 $DBC_{R/MC}$s (black), and 5 DBC_Rs (red) in H-IOP mice [population R_{max} (mean ± SE) for $HBC_{R/MC}$, $DBC_{R/MC}$, and DBC_R responses: 13 ± 4 pA, 20 ± 8 pA, and 23 ± 10 pA] are shown as dotted curves, whereas the corresponding R-Log I relations obtained from 7 $HBC_{R/MC}$s, 6 $DBC_{R/MC}$s, and 11 DBC_Rs in n-IOP mice [population R_{max} (mean ± SE) for $HBC_{R/MC}$, $DBC_{R/MC}$, and DBC_R responses: 13 ± 5 pA, 26 ± 10 pA, and 28 ± 12 pA] are shown as solid curves. (*D*) Bar graphs of the average thresholds (mean ± SE) of ΔI_C in n-IOP and H-IOP mouse retinas; the significance levels of the threshold differences are given by the *P* values of the *t* test.

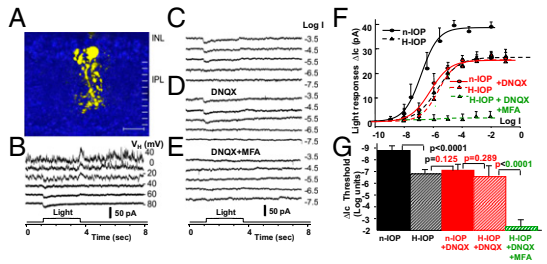

Fig. 5. Light responses of AIIACs in H-IOP and n-IOP mice. (*A–E*) Confocal image of LY-filled AIIACs in an H-IOP mouse (*A*) and its current–voltage (I-V) responses (*B*) and cation current responses to 500-nm light steps of various intensities in control solution (*C*), in the presence of 100 μM DNQX (*D*), and in the presence of 100 μM DNQX + 100 μM MFA (*E*). (*F*) Average R-Log I relations (mean ± SE) measured under various conditions in H-IOP mice are plotted as dashed curves (black, control solution, $n = 6$; red, DNQX, $n = 5$; green, DNQX+MFA, $n = 3$), and the average R-Log I relations in control solution and in DNQX in n-IOP mice are plotted as solid curves (black, control solution, $n = 15$; red, DNQX, $n = 11$). (*G*) Bar graphs of the average thresholds (mean ± SE) in n-IOP and H-IOP mice; the significance levels of the threshold differences are given by the *P* values of the *t* test. (Scale bar, *A*: 20 μm.)

DNQX to block the DBC_R→AIIAC glutamatergic synaptic inputs (34, 35, 51, 52) (Fig. 5*D*). DNQX substantially reduced the response amplitude and sensitivity of the AIIACs in the n-IOP mice (red solid R-Log I curve in Fig. 5*F*) (34) but does not significantly alter the AIIAC response amplitude and sensitivity of the AIIAC in the H-IOP mice (Fig. 5 *C* and *D* and the dashed red curve in Fig. 5*F*), suggesting that AIIACs in the H-IOP retinas have very little DBC_R input. Application of 100 μM MFA almost completely abolished the AIIAC response in the H-IOP retinas (Fig. 5*E* and green dashed curve in Fig. 5*F*), indicating that the responses in H-IOP mice are mediated by DBC_C inputs, because it has been shown that the Cx36/DBC_C-mediated responses in AIIACs are very similar to the DNQX-resistant responses (34). Our results suggest that elevated IOP suppresses AIIAC response sensitivity by mainly affecting the DBC_R→AIIAC synapses. The H-IOP–induced sensitivity decrease of DBC_R→AIIAC signals is likely to be mediated by suppression of synaptic efficacy, rather than by changes in the DBC_R output synapses to AIIACs.

Discussion

Suppression of the Rod BC Inputs to AIIACs Is a Primary Cause of Light Response Sensitivity Decrease of Retinal Ganglion Cells. In this study, we provide evidence demonstrating that elevated IOP in experimental glaucoma mouse models significantly decreases light-evoked spike response sensitivity of ONαGCs and OFFαGCs (i.e., raises thresholds by 1.5–2.5 log units), and that the decrease is primarily caused by a sensitivity reduction of ON cone bipolar cell ($DBC_{R/MC}$) signals to the ONαGCs (ΔI_C) and a sensitivity reduction of amacrine cell signals to the sOFFαGCs (ΔI_{Cl}). We also show that the soma responses of the ON and OFF bipolar cells presynaptic to ONαGCs and sOFFαGCs ($DBC_{R/MC}$s and $HBC_{R/MC}$s, respectively) (41, 53) are not significantly altered by elevated IOP but that the sensitivity of the output signals of the $DBC_{R/MC}$ axon terminals to ONαGCs (ΔI_C; synapse 3 in Fig. 1, *Right*) is significantly reduced. This may suggest that somas and axon terminals of $DBC_{R/MC}$s are not isopotential and that the high $DBC_{R/MC}$ soma sensitivity may reflect rod inputs to the dendrites of these cells (33). Anatomical and physiological evidence has suggested that AIIACs make electrical synaptic contacts with $DBC_{R/MC}$ synaptic terminals (synapse 2 in Fig. 1) (47, 54), and that the AIIAC inputs to $DBC_{R/MC}$ synaptic terminals contribute to the $DBC_{R/MC}$ outputs to ONαGCs (ΔI_C; via synapses 2 and 3 in Fig. 1) (41). Therefore, it is possible that the sensitivity reduction of $DBC_{R/MC}$ output signals to ONαGCs in H-IOP mice is mediated by the AIIACs, which send light responses of lower sensitivity to $DBC_{R/MC}$ axon terminals, resulting in an output signal (ΔI_C) of reduced sensitivity. Our observation that ΔI_{Cl} in ONαGCs was not significantly reduced by H-IOP suggests that AIIAC inputs to other ACs that make inhibitory synapses on ONαGCs are relatively minor. It has also been suggested that AIIACs make inhibitory chemical synapses onto OFFαGC dendrites (synapse 5 in Fig. 1) (44, 50, 55), and thus the H-IOP–induced sensitivity reduction of ΔI_{Cl} in sOFFαGCs may also be mediated by AIIACs. Our result in Fig. 5 shows that elevated IOP indeed reduces AIIAC response sensitivity by about 2 log units, supporting the assertion that the H-IOP–induced sensitivity loss in ON and OFF αGCs is mediated by AIIACs. Although anatomical studies have also indicated that AIIACs make chemical synapses on HBC axon terminals (47), our results that ΔI_C in OFFαGCs is less affected than ΔI_{Cl} by H-IOP are consistent with the notion that AIIAC feedback synapses on HBCs are weaker than the feedforward synapses on OFFGCs (40, 44). The single-cell AIIAC, ON, and OFFαGC results in this report are also consistent with the observation that elevated IOP reduces the voltage gains (ratio of post/presynaptic signals) of the positive and negative scotopic threshold responses (representing the GC and AIIAC responses, respectively) in living mice (12).

Experiments in Fig. 5 indicate that the reduction of AIIAC response sensitivity is primarily mediated by suppression of the rod BC (DBC_R) inputs to AIIACs (synapse 1 in Fig. 1), because the average AIIAC light responses in H-IOP mice were shifted to the same level as the average AIIAC responses of the n-IOP mice when DBC_R inputs were blocked by DNQX (black dashed curve and solid red curve in Fig. 5*F*). The average light-evoked current responses of the DBC_Rs in H-IOP mice do not significantly differ from DBC_R responses in n-IOP mice (solid and dashed red curves in Fig. 4*C*), suggesting that the reduction of AIIAC response sensitivity is not mediated by decrease of DBC_Rs' soma responses but by the efficacy of the DBC_R output synapses to AIIACs. Our observation that no significant morphological changes occur in H-IOP mice within the period of our study suggests that the changes in synaptic efficacy are mediated by physiological factors, rather than the reduction of numbers of DBC_R axon terminals or synaptic contacts. One possible element mediating such physiological changes is the BK channel in A17 amacrine cell dendritic varicosities that make feedback synapses to DBC_Rs at the axon terminal dyads (56). BK channels are known to be mechanosensitive (57), and thus chronic elevation of IOP may affect these channels and impede the efficacy of the DBC_R→AIIAC synapses. It is also interesting to note that the DBC_R→AIIAC and A17AC→DBC_R synapses are among the most proximally located chemical synapses in the mammalian retina (47, 58), and thus they may be most susceptible to chronic high IOP.

Sensitivity Loss in Inner Retinal Neurons Occurs Before Observable Structural Damage, and Thus It Is a Useful Early Diagnostic Tool for Glaucoma at Its Reversible Stages. Our results have shown that functional changes of the DBC_R→AIIAC synapses are likely to be a primary source of RGC sensitivity loss in mice with elevated IOP. We found such sensitivity reduction in ON and OFF αGCs as well as in AIIACs in mice with elevated IOP at stages before significant RGC or optic nerve degeneration is observed (12, 16). This suggests that physiological response changes may occur before structural damage in early stages of glaucoma, and thus measuring RGC and AIIAC response sensitivity changes may be used as a diagnostic tool for glaucoma at its early stages before any irreversible structural damage occurs. It is possible, for example, to develop new human scotopic optokinetic response apparatuses to screen patients with early signs of glaucoma and to determine whether therapeutic treatments are needed before

RGC/optic nerve damage and/or visual field defects are detected. From our finding that defective $DBC_R \rightarrow$AIIAC signal transmission is a primary source of sensitivity loss in inner retinal neurons, functionally repairing the $DBC_R \rightarrow$AIIAC synapses, such as targeted expression of specific synaptic proteins, ion channels [e.g., BK channels in A17 ACs (56)], and neurotrophins [e.g., BDNF (59, 60)] capable of restoring the efficacy of the $DBC_R \rightarrow$AIIAC synapses, may be a useful preventive strategy against glaucomatous degeneration. Although a large amount of work is needed to identify these synaptic molecular targets, by determining synaptic sites most vulnerable to functional changes our study provides useful information in narrowing down the scope of such a research endeavor.

Materials and Methods

Preparations. The wild-type mouse used in this project was the C57BL6J from the Jackson Laboratory. All animals were handled in accordance with Baylor College of Medicine's policies on the treatment of laboratory animals and conform to the Association for Research in Vision and Ophthalmology Statement on the Use of Animals in Ophthalmic and Vision Research and the NIH *Guide for the Care and Use of Laboratory Animals* (61). Mice were dark-adapted for 1–2 h before the experiment. To maintain the retina in the fully dark-adapted state, all further procedures were performed under infrared illumination with dual-unit Nitemare (B.E. Meyers) infrared scopes. Animals were killed by a lethal injection of ketamine + xylazine + acepromazine (0.1 mL, 100 mg/mL), and the eyes were immediately enucleated and placed in oxygenated Ames medium (Sigma) at 32–35 °C. Dissection and preparation of living retinal slices essentially followed the procedures described in previous publications (37, 40, 62, 63). All pharmacological agents (purchased from Sigma) were dissolved in Ames medium with a superfusion time of 45–80 s, and the superfusion and puff drug application procedures were described in previous publications (64–66). We found that a high dose has devastating side effects on the retina, and thus carefully calibrated the dose and found that 100 μM suppresses the gap junction and enables partial recovery after washing in retinal slices. This dose was used in tiger salamander retinal slices (67) and in mouse retinal slices in this study.

Ocular hypertension were induced on the right eye of the C57BL6J mouse line with one of two methods, as follows. (*i*) Microbead occlusion method: Six-week-old C57BL6J mice were anesthetized with weight-based i.p. injection of ketamine (80 mg/kg), xylazine (16 mg/kg), and acepromazine (1.2 mg/kg). Detailed procedures of this method are described in our previous publication (12). (*ii*) Laser/cautery coagulation method: Six-week-old C57BL6J mice were anesthetized the same way as described in the first method. One eye per animal underwent argon laser coagulation of the episcleral and limbal veins. Detailed procedures of this method are described in our previous publications (16, 68). Both methods induced sustained high IOP for over 2 mo, although RGC degeneration in eyes treated with the first method appeared at an earlier time (5–6 wk after treatment) than in eyes treated with the second method (8–12 wk after treatment) (12, 16). To assess GC, AIIAC, and BC sensitivity loss before substantial GC degeneration, all cells in this study were recorded from eyes with elevated IOP for 3–4 wk treated with the laser method or from eyes with elevated IOP for 6–7 wk treated with the microbead method. IOP was measured with a TonoLab rodent tonometer (TioLat) when the mice were anesthetized (one drop of topical proparacaine 1% solution was applied to each eye and IOP was measured 10 times). IOP was again measured at week 1 after treatment and again weekly through week 8 using the same technique. IOP measurements were averaged at each time point to establish a curve of IOP change compared with untreated fellow eyes.

Recordings, Cell Morphology, and Immunocytochemistry. Whole-cell voltage-clamp and loose-patch experiments were carried out using the Axon MultiClamp 700A amplifier connected to a Digidata 1200 interface and pClamp 10 software (Axon Instruments); the procedures for making whole-cell patch, loose-patch, and gramicidin-filled perforated patch pipettes, as well as estimation of the liquid junction potentials, have been described in previous papers (40, 64, 65). The internal solution (with 0.8 mM Lucifer yellow and/or 0.8 mM neurobiotin) for standard whole-cell patch-clamp pipettes and the external Ames medium yielded an E_{Cl} of about −60 mV. Three-dimensional cell morphology in retinal slices and flat-mounted retinas was visualized through the use of LY fluorescence or NB-conjugated fluorescence with a confocal microscope (Zeiss; 510). The procedures of *z*-axis rotation and preparation of vertical sections for cells in the flat-mounted retinas are described in an earlier publication (40). Consecutive confocal images (with optical section thickness of about 0.75 μm) were used to identify possible synaptic contact regions between two labeled neurons. Procedures of immunostaining (anti-PKCα) and subsequent processing and viewing have been described in our previous publications (33, 40, 69, 70).

Light Stimulation. The retinal slices and flat-mounted retinas were stimulated with a photostimulator that delivers light spots of various wavelengths and intensities to the retina via the epiilluminator of the microscope. Because we delivered an uncollimated stimulus light beam through an objective lens with large numerical aperture (Zeiss; 40×/0.75 water), the incident light entered the retinal slice from many directions, and thus the effect of photoreceptor self-screening was minor (71). The intensity of unattenuated 500-nm light (log I 0) is 1.4×10^6 photons·μm^{-2}·s^{-1}. The number of photoisomerizations per rod per second was calculated by using a rod cross-section of 0.45 μm^{-2} (72, 73). The light-evoked responses were plotted against light stimulus intensity, and data points were fitted by the Hill equation, $R/R_{max} = 0.5[1 + tanh\ 1.15N(Log\ I - Log\ \sigma)]$, where R is the current response amplitude, R_{max} is the maximum response amplitude, σ is the light intensity that elicits a half-maximal response, and N is the Hill coefficient (74, 75). Normalization was done cell by cell: R_{max} of each cell was set to unity, and the % responses to a given light intensity of a given group of cells were averaged and fitted by the Hill equation. Response thresholds are defined as the light intensity that generates 5% of the maximum responses. For current responses of OFF/ON GCs, AIIACs, and BCs, the peak sustained outward/inward currents (in light) compared with the baseline current (before light) were measured. For the spike response of OFF/ON GCs, the spike decrement/increment during light (number of spikes per second in light − number of spikes per second before light) was measured. Significance in threshold differences between various groups of responses (P values) was computed by the Student's t test. The intensity of light beams was calibrated with a radiometric detector (United Detector Technology).

ACKNOWLEDGMENTS. We thank Ching-Kang Jason Chen and Roy Jacoby for critically reading this manuscript, and Rob Seilheimer and Jasdeep Sabharwal for running the t tests. This work was supported by grants from the NIH (EY004446, EY019908, EY021479), NIH Vision Core (EY002520), Retina Research Foundation (Houston), and Research to Prevent Blindness.

1. Quigley HA, Broman AT (2006) The number of people with glaucoma worldwide in 2010 and 2020. *Br J Ophthalmol* 90(3):262–267.
2. Gordon MO, et al. (2002) The Ocular Hypertension Treatment Study: Baseline factors that predict the onset of primary open-angle glaucoma. *Arch Ophthalmol* 120(6): 714–720, discussion 829–830.
3. Quigley HA, Green WR (1979) The histology of human glaucoma cupping and optic nerve damage: Clinicopathologic correlation in 21 eyes. *Ophthalmology* 86(10): 1803–1830.
4. Lee BL, et al. (1998) The Glaucoma Symptom Scale. A brief index of glaucoma-specific symptoms. *Arch Ophthalmol* 116(7):861–866.
5. Quigley HA (1995) Ganglion cell death in glaucoma: Pathology recapitulates ontogeny. *Aust N Z J Ophthalmol* 23(2):85–91.
6. Mittag TW, et al. (2000) Retinal damage after 3 to 4 months of elevated intraocular pressure in a rat glaucoma model. *Invest Ophthalmol Vis Sci* 41(11):3451–3459.
7. Howell GR, et al. (2007) Axons of retinal ganglion cells are insulted in the optic nerve early in DBA/2J glaucoma. *J Cell Biol* 179(7):1523–1537.
8. John SW, Harder JM, Fingert JH, Anderson MG (2014) Animal models of exfoliation syndrome, now and future. *J Glaucoma* 23(8, Suppl 1):S68–S72.
9. Anderson D (1987) Visual field loss in glaucoma. *Perimetry With and Without Automation*, ed Anderson DR (Mosby, St. Louis), pp 142–159.
10. Henson DB, Artes PH, Chauhan BC (1999) Diffuse loss of sensitivity in early glaucoma. *Invest Ophthalmol Vis Sci* 40(13):3147–3151.
11. Wilensky JT, Hawkins A (2001) Comparison of contrast sensitivity, visual acuity, and Humphrey visual field testing in patients with glaucoma. *Trans Am Ophthalmol Soc* 99:213–217, discussion 217–218.
12. Frankfort BJ, et al. (2013) Elevated intraocular pressure causes inner retinal dysfunction before cell loss in a mouse model of experimental glaucoma. *Invest Ophthalmol Vis Sci* 54(1):762–770.
13. Drum B, Armaly MF, Huppert W (1986) Scotopic sensitivity loss in glaucoma. *Arch Ophthalmol* 104(5):712–717.
14. Glovinsky Y, Quigley HA, Drum B, Bissett RA, Jampel HD (1992) A whole-field scotopic retinal sensitivity test for the detection of early glaucoma damage. *Arch Ophthalmol* 110(4):486–490.
15. Leske MC, et al.; Early Manifest Glaucoma Trial Group (2003) Factors for glaucoma progression and the effect of treatment: The early manifest glaucoma trial. *Arch Ophthalmol* 121(1):48–56.

16. Ji J, et al. (2005) Effects of elevated intraocular pressure on mouse retinal ganglion cells. *Vision Res* 45(2):169–179.
17. Buckingham BP, et al. (2008) Progressive ganglion cell degeneration precedes neuronal loss in a mouse model of glaucoma. *J Neurosci* 28(11):2735–2744.
18. McKinnon SJ, Schlamp CL, Nickells RW (2009) Mouse models of retinal ganglion cell death and glaucoma. *Exp Eye Res* 88(4):816–824.
19. Bui BV, Fortune B (2004) Ganglion cell contributions to the rat full-field electroretinogram. *J Physiol* 555(Pt 1):153–173.
20. John SW, et al. (1998) Essential iris atrophy, pigment dispersion, and glaucoma in DBA/2J mice. *Invest Ophthalmol Vis Sci* 39(6):951–962.
21. Della Santina L, Inman DM, Lupien CB, Horner PJ, Wong RO (2013) Differential progression of structural and functional alterations in distinct retinal ganglion cell types in a mouse model of glaucoma. *J Neurosci* 33(44):17444–17457.
22. Harwerth RS, et al. (2002) Visual field defects and neural losses from experimental glaucoma. *Prog Retin Eye Res* 21(1):91–125.
23. Soto I, et al. (2008) Retinal ganglion cells downregulate gene expression and lose their axons within the optic nerve head in a mouse glaucoma model. *J Neurosci* 28(2): 548–561.
24. Libby RT, et al. (2005) Inherited glaucoma in DBA/2J mice: Pertinent disease features for studying the neurodegeneration. *Vis Neurosci* 22(5):637–648.
25. Inman DM, Sappington RM, Horner PJ, Calkins DJ (2006) Quantitative correlation of optic nerve pathology with ocular pressure and corneal thickness in the DBA/2 mouse model of glaucoma. *Invest Ophthalmol Vis Sci* 47(3):986–996.
26. Jakobs TC, Libby RT, Ben Y, John SW, Masland RH (2005) Retinal ganglion cell degeneration is topological but not cell type specific in DBA/2J mice. *J Cell Biol* 171(2): 313–325.
27. Holcombe DJ, Lengefeld N, Gole GA, Barnett NL (2008) Selective inner retinal dysfunction precedes ganglion cell loss in a mouse glaucoma model. *Br J Ophthalmol* 92(5):683–688.
28. Sappington RM, Carlson BJ, Crish SD, Calkins DJ (2010) The microbead occlusion model: A paradigm for induced ocular hypertension in rats and mice. *Invest Ophthalmol Vis Sci* 51(1):207–216.
29. Abd-El-Barr MM, et al. (2009) Genetic dissection of rod and cone pathways in the dark-adapted mouse retina. *J Neurophysiol* 102(3):1945–1955.
30. Saszik SM, Robson JG, Frishman LJ (2002) The scotopic threshold response of the dark-adapted electroretinogram of the mouse. *J Physiol* 543(Pt 3):899–916.
31. Baltan S, et al. (2010) Metabolic vulnerability disposes retinal ganglion cell axons to dysfunction in a model of glaucomatous degeneration. *J Neurosci* 30(16):5644–5652.
32. Porciatti V, Saleh M, Nagaraju M (2007) The pattern electroretinogram as a tool to monitor progressive retinal ganglion cell dysfunction in the DBA/2J mouse model of glaucoma. *Invest Ophthalmol Vis Sci* 48(2):745–751.
33. Pang JJ, et al. (2010) Direct rod input to cone BCs and direct cone input to rod BCs challenge the traditional view of mammalian BC circuitry. *Proc Natl Acad Sci USA* 107(1):395–400.
34. Pang JJ, et al. (2007) Relative contributions of rod and cone bipolar cell inputs to AII amacrine cell light responses in the mouse retina. *J Physiol* 580(Pt 2):397–410.
35. Trexler EB, Li W, Massey SC (2005) Simultaneous contribution of two rod pathways to AII amacrine and cone bipolar cell light responses. *J Neurophysiol* 93(3):1476–1485.
36. Wässle H, Puller C, Müller F, Haverkamp S (2009) Cone contacts, mosaics, and territories of bipolar cells in the mouse retina. *J Neurosci* 29(1):106–117.
37. Pang JJ, Gao F, Wu SM (2004) Light-evoked current responses in rod bipolar cells, cone depolarizing bipolar cells and AII amacrine cells in dark-adapted mouse retina. *J Physiol* 558(Pt 3):897–912.
38. Pang JJ, Gao F, Wu SM (2012) Physiological characterization and functional heterogeneity of narrow-field mammalian amacrine cells. *J Physiol* 590(Pt 1):223–234.
39. Pang JJ, Gao F, Paul DL, Wu SM (2012) Rod, M-cone and M/S-cone inputs to hyperpolarizing bipolar cells in the mouse retina. *J Physiol* 590(Pt 4):845–854.
40. Pang JJ, Gao F, Wu SM (2003) Light-evoked excitatory and inhibitory synaptic inputs to ON and OFF alpha ganglion cells in the mouse retina. *J Neurosci* 23(14):6063–6073.
41. Schwartz GW, et al. (2012) The spatial structure of a nonlinear receptive field. *Nat Neurosci* 15(11):1572–1580.
42. Murphy GJ, Rieke F (2006) Network variability limits stimulus-evoked spike timing precision in retinal ganglion cells. *Neuron* 52(3):511–524.
43. Wang YV, Weick M, Demb JB (2011) Spectral and temporal sensitivity of cone-mediated responses in mouse retinal ganglion cells. *J Neurosci* 31(21):7670–7681.
44. Arman AC, Sampath AP (2012) Dark-adapted response threshold of OFF ganglion cells is not set by OFF bipolar cells in the mouse retina. *J Neurophysiol* 107(10):2649–2659.
45. Doi M, Uji Y, Yamamura H (1995) Morphological classification of retinal ganglion cells in mice. *J Comp Neurol* 356(3):368–386.
46. Peichl L (1989) Alpha and delta ganglion cells in the rat retina. *J Comp Neurol* 286(1): 120–139.
47. Chun MH, Han SH, Chung JW, Wässle H (1993) Electron microscopic analysis of the rod pathway of the rat retina. *J Comp Neurol* 332(4):421–432.
48. Veruki ML, Hartveit E (2009) Meclofenamic acid blocks electrical synapses of retinal AII amacrine and on-cone bipolar cells. *J Neurophysiol* 101(5):2339–2347.
49. Pan F, Mills SL, Massey SC (2007) Screening of gap junction antagonists on dye coupling in the rabbit retina. *Vis Neurosci* 24(4):609–618.
50. Manookin MB, Beaudoin DL, Ernst ZR, Flagel LJ, Demb JB (2008) Disinhibition combines with excitation to extend the operating range of the OFF visual pathway in daylight. *J Neurosci* 28(16):4136–4150.
51. Singer JH (2007) Multivesicular release and saturation of glutamatergic signalling at retinal ribbon synapses. *J Physiol* 580(Pt 1):23–29.
52. Singer JH, Diamond JS (2006) Vesicle depletion and synaptic depression at a mammalian ribbon synapse. *J Neurophysiol* 95(5):3191–3198.
53. Wu SM, Gao F, Pang JJ (2004) Synaptic circuitry mediating light-evoked signals in dark-adapted mouse retina. *Vision Res* 44(28):3277–3288.
54. Veruki ML, Hartveit E (2002) AII (rod) amacrine cells form a network of electrically coupled interneurons in the mammalian retina. *Neuron* 33(6):935–946.
55. Münch TA, et al. (2009) Approach sensitivity in the retina processed by a multifunctional neural circuit. *Nat Neurosci* 12(10):1308–1316.
56. Grimes WN, Li W, Chávez AE, Diamond JS (2009) BK channels modulate pre- and postsynaptic signaling at reciprocal synapses in retina. *Nat Neurosci* 12(5):585–592.
57. Irnaten M, et al. (2013) Elevated maxi-K^+ ion channel current in glaucomatous lamina cribrosa cells. *Exp Eye Res* 115:224–229.
58. Brandstätter JH, Löhrke S, Morgans CW, Wässle H (1996) Distributions of two homologous synaptic vesicle proteins, synaptoporin and synaptophysin, in the mammalian retina. *J Comp Neurol* 370(1):1–10.
59. Gupta V, et al. (2014) BDNF impairment is associated with age-related changes in the inner retina and exacerbates experimental glaucoma. *Biochim Biophys Acta* 1842(9): 1567–1578.
60. Iuvone PM, Boatright JH, Tosini G, Ye K (2014) *N*-acetylserotonin: Circadian activation of the BDNF receptor and neuroprotection in the retina and brain. *Adv Exp Med Biol* 801:765–771.
61. Committee for the Update of the *Guide for the Care and Use of Laboratory Animals* (2011) *Guide for the Care and Use of Laboratory Animals* (National Academies Press, Washington, DC), 8th Ed.
62. Wu SM (1987) Synaptic connections between neurons in living slices of the larval tiger salamander retina. *J Neurosci Methods* 20(2):139–149.
63. Werblin FS (1978) Transmission along and between rods in the tiger salamander retina. *J Physiol* 280(1):449–470.
64. Gao F, Maple BR, Wu SM (2000) I4AA-sensitive chloride current contributes to the center light responses of bipolar cells in the tiger salamander retina. *J Neurophysiol* 83(6):3473–3482.
65. Maple BR, Wu SM (1998) Glycinergic synaptic inputs to bipolar cells in the salamander retina. *J Physiol* 506(Pt 3):731–744.
66. Zhang AJ, Jacoby R, Wu SM (2011) Light- and dopamine-regulated receptive field plasticity in primate horizontal cells. *J Comp Neurol* 519(11):2125–2134.
67. Zhang AJ, Wu SM (2009) Receptive fields of retinal bipolar cells are mediated by heterogeneous synaptic circuitry. *J Neurosci* 29(3):789–797.
68. Gross RL, et al. (2003) A mouse model of elevated intraocular pressure: Retina and optic nerve findings. *Trans Am Ophthalmol Soc* 101:163–169, discussion 169–171.
69. Pang JJ, Wu SM (2011) Morphology and immunoreactivity of retrogradely double-labeled ganglion cells in the mouse retina. *Invest Ophthalmol Vis Sci* 52(7):4886–4896.
70. Zhang J, Yang Z, Wu SM (2005) Development of cholinergic amacrine cells is visual activity-dependent in the postnatal mouse retina. *J Comp Neurol* 484(3):331–343.
71. Field GD, Rieke F (2002) Mechanisms regulating variability of the single photon responses of mammalian rod photoreceptors. *Neuron* 35(4):733–747.
72. Howes KA, et al. (2002) GCAP1 rescues rod photoreceptor response in GCAP1/GCAP2 knockout mice. *EMBO J* 21(7):1545–1554.
73. Luo DG, Yau KW (2005) Rod sensitivity of neonatal mouse and rat. *J Gen Physiol* 126(3):263–269.
74. Thibos LN, Werblin FS (1978) The properties of surround antagonism elicited by spinning windmill patterns in the mudpuppy retina. *J Physiol* 278(1):101–116.
75. Yang XL, Wu SM (1996) Response sensitivity and voltage gain of the rod- and cone-horizontal cell synapses in dark- and light-adapted tiger salamander retina. *J Neurophysiol* 76(6):3863–3874.